The Engine Reformer: Syngas Production in an Engine for Compact Gas-to-Liquids Synthesis

Emmanuel G. Lim, Enoch E. Dames, Angela J. Acocella, Thomas R. Needham, Andrea Arce, Daniel Cohn, Leslie Bromberg, Wai K. Cheng, William H. Green*

Abstract

Methane (CH_4) reforming was carried out in an internal combustion engine (an "engine reformer"). We successfully produced syngas from the partial oxidation of natural gas in the cylinder of a diesel engine that was reconfigured to perform spark ignition. Performing the reaction in an engine cylinder allows some of the exothermicity to be captured as useful work. Intake conditions of 1.1 bar and up to 480 °C allowed low cycle-to-cycle variability (COV_{nimep} < 20%) at methane-air equivalence ratios (ϕ_M) of 2.0, producing syngas with an H_2 to CO ratio of 1.4. Spark ignition timing was varied between 45° and 30° before top-dead-center (BTDC) piston position, showing significant improvement with delayed timing. Hydrogen (H_2) and ethane (C_2H_6) were added to simulate recycle from a downstream synthesis reactor and realistic natural gas compositions, respectively. Addition of these gases yielded stable combustion up to hydrocarbon-air equivalence ratios (ϕ_{HC}) of 2.8 with COV_{nimep} < 5%. Ethane concentrations with respect to methane of up to 20% by volume (with and without H_2) produced robust and stable combustion, demonstrating that the engine can be operated across a range of natural gas compositions. Engine exhaust soot concentrations demonstrated elevated values at ϕ_{HC} > 2.4, but < 1 mg/L below these equivalence ratios. These results demonstrate that the engine reformer could be a key component of a compact gas-to-liquids synthesis plant by highlighting the operating conditions under which high gas conversion, high H_2 to CO ratios close to 2.0, and low soot production are possible.

Keywords

Gas-to-liquids, engine, syngas, methane, partial oxidation

* Corresponding author. *E-mail address*: whgreen@mit.edu

Introduction

The Need for Compact GTL

There is a need for Gas-to-Liquids (GTL) plants that can serve stranded natural gas sources, since there are currently no economical ways to send that gas to market. Economic factors drive whether gas should be extracted, left in the ground, burned as waste, or in this case, converted to a liquid fuel. When gas transportation costs are too high, that gas is either abandoned and deemed "stranded", or it is flared as in the case of associated gas[1]. Compression or liquefaction are both expensive means to treat gas for transport. However, conversion to a liquid fuel could allow this gas to be transported economically. In conditions where the output of natural gas is small, there are few options other than to flare. In North Dakota alone, over one third of natural gas production was flared in 2011. [1] Throughout the United States, flaring is significant at associated gas sites, and the majority of associated gas wells produced 0.4 – 1.5 mmscfd of natural gas in 2009. [2] This gas production rate is poorly matched to existing GTL plants, which process three orders of magnitude more gas. The technology used in large-capacity GTL plants cannot serve individual or small groups of wells because of reverse economies of scale if they were reduced in size. Also, the gas production rate from many wells drops off in a few years, while conventional GTL plants are built to last for decades. A small-scale GTL unit which could be moved to a new location as desired would be particularly useful for processing associated gas.

There is therefore a strong interest in developing compact GTL technologies that can integrate a synthesis gas ("syngas") production unit, liquid fuel synthesis reactor, and compressors in a small footprint, in order to synthesize liquid fuels such as methanol that are significantly cheaper to transport than natural gas. The present challenge is in making the syngas production unit economical on a small scale, as it comprises the majority of the capital cost of large-scale GTL plants. For example, to produce dimethyl ether (DME) from syngas-derived methanol on a large scale, syngas production accounts for 60% of capital costs, while the remaining 40% can be attributed to liquids synthesis. [3] On a small scale, this cost distribution may in fact be even less favorable for the syngas production step if using conventional technologies, and this is where the engine reformer can provide a solution.

Current Technologies

Non-catalytic partial oxidation of natural gas is a well-studied technology for the large-scale production of syngas. Technologies based on the Shell and Texaco Gasification processes operate in excess of 1000 °C and 35 bar. [4] Plants based on these technologies require high throughputs to be economical and may only be applied where gas is available in large quantities. However, since the same temperature and pressure conditions are reached in an engine cylinder, the same chemistry may be performed on a much smaller scale. Furthermore, depending on the size of the engine cylinder and the

[1] Associated gas is natural gas released when crude oil is extracted. If the cost to transport that gas to market is prohibitive, it is typically flared.

total number of cylinders, the total gas processing flow rate can be tailored to match the gas source.

Catalytic routes to partial oxidation of methane are also possible with transition metal or noble metal catalysts. Experiments have been performed at 1 atm and 673-1273 K with CH_4 and pure O_2 or air using Ni and/or Co transition metals, or Ir, Pt, Pd, Ru, Rh noble metal catalysts. [5] Lower temperatures and pressures necessary to achieve high conversion rates are a major draw for the catalytic route, though questions still remain about catalyst stability and lifetime. The economics of these technologies are also bound by the high capital investment required to operate on a small scale, while an engine performing non-catalytic partial oxidation may not be constrained in the same way. [6]

Conventional GTL technologies are only economical on a large scale. For example, the Shell Pearl GTL plant in Qatar produces 140,000 barrels of oil equivalent per day (boe/d) of GTL products. [7] Large plants, especially on the scale of Shell Pearl, are associated with long construction times and cost escalation over time. Market conditions can change substantially during the construction period, increasing the economic risks. Furthermore, these technologies do not scale favorably to small scale, and novel approaches are being investigated in this paper to address natural gas sources such as associated gas that are either small or have short production periods. To illustrate the cost improvement, the capital cost of large methanol plants are estimated to be $700 / MT/yr, [8] while a 30 ton per day methanol plant using an engine reformer to produce syngas is projected to cost $360 / MT/yr. [6]

There are several small-scale GTL approaches that are being attempted today. They are described in Table 1, demonstrating the difference in gas processing capacity between small and large scale. An important factor to the success of small-scale plants is how close the plant capacity can be to production rates at associated gas sites. The typical associated gas well in the United States produced 0.4 – 1.5 mmscfd of natural gas in 2009. [2]

Table 1. Natural gas processing capacities of existing GTL projects.

Company	Scale	Natural Gas Processing Capacity (mmscfd)	Source
Oberon	Small	1.240	[9]
Hydrochem	Small	1.968	[10]
Gas Technologies	Small	30.000	[11]
Shell (Pearl)	Large	1,600.000	[7]

The Engine Reformer

We have been investigating the possibility of using slightly modified engines for the production of hydrogen rich gas from methane (CH_4), by combusting CH_4 in the engine under extremely fuel-rich regimes. This can promote partial oxidation (POX) to produce syngas, and can therefore be used in tandem with a liquids synthesis reactor to make liquid fuels such as methanol.

The main role of the internal combustion engine in today's society is for the production of power by converting chemical energy in fuel, to useful work. In a conventional engine, complete combustion of a fuel such as CH_4 is desired to maximize combustion efficiency and minimize hydrocarbon emissions. The products of complete combustion are carbon dioxide (CO_2) and water (H_2O) as illustrated in Eq. 1. In the work presented in this paper, we instead treat the engine as a chemical reactor for the production of syngas, a necessary precursor in the synthesis of longer chain hydrocarbons such as fuels produced by the Fischer-Tropsch method, or methanol. [12] In order to produce syngas, we operate the engine in an O_2-starved environment (fuel-rich) in order to partially oxidize CH_4, thereby generating H_2 and CO as shown in Eq. 2. When coupled with a liquids synthesis reactor (Fig. 1), the engine reformer may be deployed to convert stranded gas into liquid products, which are easier to transport.

$$CH_4 + 2\,O_2 \leftrightarrow CO_2 + 2\,H_2O \qquad \Delta H^{\circ}_{298} = -802 \text{ kJ/mol} \tag{1}$$

$$CH_4 + 0.5\,O_2 \leftrightarrow CO + 2\,H_2 \qquad \Delta H^{\circ}_{298} = -36 \text{ kJ/mol} \tag{2}$$

Because of the industrial application of the engine reformer, a good fraction of the literature occurs in patents. Four relevant patents have been filed for the partial oxidation of methane in an engine. Three of those four are expired. They are US 2543791 A [13] by Texas Co (filed August 25, 1949), US 2846297 A [14] by Maschinenfabrik Augsburg (filed October 8, 1954), US 2922809 A [15] by Sun Oil Co (filed December 13, 1957) and US 20140144397 [16] by MIT (filed March 14, 2013). Texas Co claims to prevent irregular engine operation and misfire by separately introducing fuel (or steam) first, then oxidant, into the cylinder. Residual gases are prevented from combusting by scavenging the residuals with fuel or steam before oxygen is introduced. Maschinenfabrik Augsburg describes an operating procedure for synthesis gas production in an engine, where stoichiometric mixtures are fed to the engine during start-up until an appropriate engine temperature is reached before richer fuel-air mixtures are allowed into the cylinder. Sun Oil Co describes a method to operate a motored engine with 20:1 to 60:1 compression ratio, with methane-oxygen equivalence ratios as high as 18 and pre-heated to 600-800 °F, resulting in peak cylinder temperatures of 1200-1400 °F. The product is an aqueous solution of heavier hydrocarbons such as acetaldehyde, acetone, dimethyl acetal, methanol, ethanol, isopropanol and formaldehyde.

The technology described in this work is protected by the fourth patent. [16] It describes a way to integrate an engine reformer into a small-scale liquids synthesis plant. It describes reusing shaft power and exhaust gas heat to heat the reactants, produce oxygen, provide electricity, or operate a compressor. Requirements for liquids synthesis are well-integrated into the design of the engine's operating regime, such as a ratio of H_2 to CO close to 2 in the exhaust. Integration with a specific synthesis technology is a unique feature of this patent, as others are vague or agnostic.

Karim et al [17–19] demonstrated partial oxidation of methane in a dual fuel engine. Experiments were carried out in a 115 mm bore, 152 mm stroke, 14.2:1 compression

ratio diesel engine at 1000 rpm and ambient intake temperature. Methane and oxygen-enriched air were fed to the engine and a small quantity of diesel was injected to trigger combustion. Fuel-air equivalence ratios up to 2.5 were tested. The higher equivalence ratios were achieved by oxygen-enrichment of air (up to 80% O_2). H_2 to CO ratios up to 1.4 were produced with these inputs. Reliable combustion at higher equivalence ratios, where combustion is less likely to occur without significant preheating, can be achieved by reducing the quantity of inert N_2 in the oxidizer. In practice, a high O_2 oxidizer concentration > 80% requires expensive air separation technology such as vacuum pressure swing adsorption (VPSA) or cryogenic air separation and should be avoided if possible to reduce capital cost, which is especially important for smaller plants.

Yamamoto et al [20] tested partial oxidation of natural gas in an 8 cylinder diesel engine with 175 mm bore, 220 mm stroke and compression ratio of 7:1 that was modified to perform spark ignition. Natural gas with 94.8% CH_4 (2.3% CO_2, 2.7% N_2, 0.2% O_2) was used, and oxygen-enriched air with 97.2% O_2 and 2.8% N_2 was used for combustion. The elimination of N_2 allowed higher flame speeds to be achieved in the cylinder. The maximum fuel-air equivalence ratio that was achieved was $\phi_{HC} = 2.5$ (O_2/CH_4 ratio of 0.8), which produced a H_2/CO ratio of 1.65, and carbon in the exhaust gas with a concentration of 0.5 g/m^3, or 0.5 mg/L. Combustion stability in these regimes was never quantified. Furthermore, like Karim, Yamamoto et al used oxygen-enriched air while in the present work, only air was used.

Other relevant results in the literature include Ghaffarpour et al, [21] who provide simulation results that show that a methane-air equivalence ratio greater than 1.4 is required to achieve an H_2/CO ratio greater than 1.0. This justifies the decision to target equivalence ratios at or above 2.0, where the production of H_2 is preferred. Also, McMillian et al [22] tested spark ignition of natural gas mixtures from fuel-to-air equivalence ratios of 0.6 to 1.6. Their testing was performed in a Ricardo Proteus single cylinder 4-stroke diesel engine with a 130 mm bore and 150 mm stroke, 1.997 L displacement volume, and compression ratio of 13.3:1. Their fuel contained 2.7% C_2H_6, 95% CH_4, with the balance in N_2 and heavier hydrocarbons. With a fuel-to-air equivalence ratio of 1.6, the H_2:CO ratio was 1.1. They performed soot detection with a 12:1 dilution ratio, with a constant flow rate of 35-40 cm/s across a 90 mm diameter soot filter. Based on the brake thermal efficiency of the engine of 19% at this equivalence ratio, where fuel flow rate was 2.63 g/s, the calculated soot concentration in their exhaust was 0.7 g/m^3, or 0.7 mg/L.

The main objective in this work is to empirically demonstrate reliable engine operation and to investigate exhaust gas composition with the following guidelines. The remainder of this paper reports on our experiments to demonstrate these goals, which illustrate the internal combustion engine's compatibility in a small-scale GTL plant for the synthesis of methanol.

- H_2 to CO ratio as close as possible to 2 to 1 in exhaust gas to reduce the demand on water-gas shift in post-processing.
- High CH_4 conversion efficiency.
- High CH_4 throughput.

- Elevated intake temperatures to increase flame speed of intake mixture and hence allow reliable combustion at high equivalence ratios.
- Investigation of the effect of spark advance on combustion, and determine optimal spark timing.
- Determination of maximum equivalence ratio with robust combustion with and without addition of H_2 or C_2H_6.
- Simulation of recycle of H_2 from downstream liquids synthesis unit by adding 5% H_2 by volume at the intake.
- Simulation of real natural gas compositions with up to 20% C_2H_6 by volume in CH_4.
- Measurement of soot concentrations in engine exhaust to evaluate performance at different equivalence ratios.

Experimental Methods

A modified Yanmar 4TNV84T diesel-injection engine[2] with 84 mm bore, 90 mm stroke and compression ratio of 18.9:1 was used. One of the 4 cylinders was converted to perform spark-ignition (the "test" cylinder). In the test cylinder, the diesel injector was removed to make room for a spark plug (NGK R847-11 surface discharge racing spark plug), and the original diesel supply line was welded and sealed. A threaded hole under the diesel injector pedestal was drilled to accommodate a Kistler 6052C high-temperature pressure sensor to measure in-cylinder pressure during combustion. A Kistler 5010 Dual Mode Amplifier amplified the pressure signal for data acquisition.

An H25 incremental optical rotary encoder from BEI Sensors was directly coupled to the engine crankshaft. This produced two out of phase square waves with 50% duty cycle and a cycle period of 1 CAD, and one square wave with peak width 0.5 CAD and cycle period 360 CAD. This third signal was timed to bottom-dead-center (BDC) piston position. All three signals were filtered by a BEI optical-isolator module. The isolated BDC signal was filtered with a Fairchild Semiconductor DM7474 positive-edge-triggered D-type flip-flop and Texas Instruments SN74LS08N positive-and gate to select compression-stroke[3] BDC and maintain consistent high-level output. Compression-stroke BDC signals were isolated for correct timing during data collection.

An off-the-shelf 1996 Dodge Caravan Mopar[4] ignition coil was used to produce the sparking voltages. An International Rectifier GB14C40L automotive ignition IGBT was used to provide the switching currents for the primary winding in the ignition coil. The switching square wave signal with correct spark timing was generated by a separate dedicated computer which read engine speed and spark timing inputs from the controlling computer, and based on bottom-dead-center (BDC) timing and crank angle degree (CAD) timing signals from the optical rotary encoder, generated a square pulse in time with each spark. This timing signal had 1 CAD resolution.

Fuel and air were mixed upstream of the test cylinder, and the test cylinder exhaust was processed separately due to high concentrations of H_2 and CO gas. Room air was drawn in for the remaining three diesel cylinders. 50% ethylene glycol in water was used as engine coolant, maintained at 95 °C throughout experimental testing. Intake gases for the test cylinder were supplied from bottled ultra high purity CH_4, H_2 and C_2H_6 from Airgas. Compressed air was provided from an Atlas Copco GA30FF oil-injected rotary screw compressor at 100 psi, regulated down to 40 psi. Test cylinder intake compositions and flow rates were controlled by four Omega FMA-2600A series mass flow controllers and one Cole-Parmer EW-32907-69, with one controller per gas type (Table 2). Flammable gases (CH_4, C_2H_6 and H_2) were mixed separately from air, and passed through a buffering chamber downstream of their respective mass flow controllers in order to reduce the effect of pressure fluctuations in the intake manifold on the controller valves. Two Omega AHPF-122 1200W air process heaters and one AHPF-082 600W air process

[2] 1.995 L; 4 cylinders; 4 valves per cylinder; four-stroke

[3] Each cycle in a four-stroke engine has four periods: compression, expansion, exhaust and intake, in that order.

[4] OEM# 04609080

heater heated air and fuel mixtures respectively. The gases were mixed in porous copper foam housed in a 1" NPT pipe wye. Intake and exhaust temperatures were measured with Omega K-type thermocouples. Intake and exhaust pressures were measured with Data Instruments Model SA 0-25 PSIA 1-5 VDC pressure transducers, one in each test manifold.

Table 2. Mass flow controller maximum flow rates were selected based on expected operating ranges for each gas.

Gas	Flow Controller Maximum Flow Rate (SLPM)
Air	250
CH_4	100
H_2	50
C_2H_6	5

A sample line was drawn from the main engine exhaust and cooled by a water jacket at 0 °C to remove water vapor. A second tee from the cooled and dried gas was drawn at 0.2 scfh by a KNF Neuberger UN726FTP diaphragm vacuum pump through a Parker 9900-05-BK Balston filter and Drierite 10-20 mesh anhydrous indicating desiccant to remove particulate matter and water vapor. This gas was analyzed in an Agilent 490 Micro GC using settings described in Table 3. The gases used for calibration are described in Table 4. GC data were collected using Agilent OpenLAB software and processed in MATLAB.

Table 3. Two columns were used in the Agilent 490 Micro GC with a thermal conductivity detector. MS5A was used to detect H_2, O_2, N_2, CH_4, CO. PPU was used to detect CO_2 and C_2H_6. Each column was operated under slightly different conditions to suit target gas detection and run times.

	Column Type	
	CP-Molsieve 5A (MS5A)	*PoraPLOT U (PPU)*
Carrier Gas	Argon	Helium
Injector Temperature (°C)	110	
Injection Time (ms)	40	
Backflush Time (s)	11	n/a
Column Temperature (°C)	80	50
Initial Pressure (kPa)	150	
Sampling Frequency (Hz)	100	
Run Time (s)	150	
Stabilizing Time (s)	5	
Sample Time (s)	90	
Sample Line Temperature (°C)	37	

Table 4. Composition of calibration gases. Bold indicates this composition was used for calibration.

Gas	*Composition*	
1	**20% CO_2**	**80% N_2**
2	**40% H_2**	60% N_2
3	**21% O_2**	79% N_2
4	**5% CH_4**	95% Ar
5	**10% CO**	90% N_2
6	**15% C_2H_6**	85% Ar

Remaining gases not used for GC testing were combusted in a Fives North American "Aardvark" high velocity burner to complete oxidation of H_2 and CO. This was performed to comply with safety regulations on CO release. A Gast Regenair R2103 regenerative blower supplied air to the burner. An Autolite 3163 spark plug provided the ignition source.

A National Instruments NI 9205 Analog Input Module and NI 9213 Thermocouple Input Module were used to collect pressure and temperature data respectively. A National Instruments NI cDAQ-9188 Ethernet chassis merged all measurement data from the input modules and collected timing signals from the logic circuit described above. Data was visualized and collected by a LabVIEW VI, which communicated with the DAQ chassis over Ethernet.

The LabVIEW program calculated mass flow rate set points for each mass flow controller, which were then communicated through RS-232 to the controllers themselves. These set points were calculated by determining the mass fraction of each compound in the gas mixture based on desired hydrocarbon-air equivalence ratio ϕ_{HC}, H_2 concentration in the total mixture x_{H_2}, and C_2H_6 concentration in the fuel mixture $x_{C_2H_6}$. The flow rate for each gas was calculated as a fraction of the total mass flow rate drawn by the engine (in g/min), which is a function of engine speed (rev/min), intake pressure p_i (kPa), intake temperature T_i (K), the Ideal Gas constant R, and and molecular weight of the mixture $\boldsymbol{M_{mix}}$ as shown in Eq. 3. The measured intake pressure was maintained at 1.1 bar in real time.

$$\dot{m}_{engine} = \frac{N\, V_d\, p_i\, M_{mix}}{2\, R\, T_i} \tag{3}$$

Engine exhaust soot concentration was measured using a gravimetric soot detection apparatus. Engine exhaust was drawn through a heated stainless steel tube by a Gast 1423 rotary vane vacuum pump. The exhaust gas samples were passed through dried Pall LifeSciences PALLFLEX 47 mm Tissuquartz™ (2500 QAT-UP) membrane filters, which were held in place by a Gelman Sciences 2220 filter holder. Water vapor was condensed from the gas by cooling it to room temperature through a counter flow heat exchanger. A constant volumetric flow rate was maintained during sampling, as measured by an Omega FVL-1611A volumetric flow meter calibrated to room air, and the time of sampling was measured in order to calculate the total sample volume. A small error will exist in the volume flow rate measurement due to the discrepancy between true and actual viscosity of the gas going through the meter at different operating points. However, since the majority of the gas is N_2 (~ 70% in the exhaust mixtures), its viscosity should not deviate significantly from that of air. Each piece of filter paper was processed in a dehumidifier for at least 24 hours prior to testing, and then weighed. After soot samples were collected, the specimens were dried again in the same dehumidifier for at least 24 hours before being weighed again. The difference between initial and final mass of each filter paper specimen was taken to determine the soot collected in that test. The collected soot mass divided by the total volume flow provided the soot concentration.

Numerical Methods

The Python 2.7 interface of Cantera [23] version 2.1.2 was used for all simulations in this work. USC Mech II [24] was used for computation of laminar premixed flame speeds and soot propensity predictions. Convergence of predicted laminar flame speed with grid size was ensured. Relative sooting propensity was determined by comparing predicted peak benzene mole fractions for varying fuel mixtures.

Results & Discussion

Calculations

The methane-air equivalence ratio (ϕ_M) is used where the fuel is composed entirely of methane. The hydrocarbon-air equivalence ratio (ϕ_{HC}) is used where methane and ethane may both be present as fuel. These ratios were modified in real-time by the mass flow controllers. Hydrogen was not considered as a fuel in either of these calculations, when it was present. This is to highlight its role as a precursor to liquids synthesis, as well as a component from recycling. For ideal partial oxidation, ϕ_M = 4 as shown in Eq. 4.

The intake composition was first defined with respect to CH_4 by the stoichiometry in Eq. 4. Based on ϕ_M in Eq. 5, the mass fraction of CH_4 and air was solved for separately, and communicated to the mass flow controllers. Being able to operate without either C_2H_6 or H_2 was critical so that the effect of adding those gases could be detected, but also in order to smoothly start up the engine. For example, to ramp up to the higher equivalence ratios made possible by higher intake temperatures, the engine was first operated at close to $\phi_M = 1.0$ to provide steady combustion at lower intake temperatures.

$$CH_4 + \frac{2}{\phi_M}\,(O_2 + 3.773\,N_2) \tag{4}$$

$$\phi_M = \frac{\left(m_{CH_4}/m_{air}\right)_{actual}}{\left(m_{CH_4}/m_{air}\right)_{stoich}} \tag{5}$$

Natural gas can contain a significant quantity of C_2H_6 and other higher hydrocarbons. We have investigated the impact on the reformer when a substantial fraction of higher hydrocarbons are present. $x_{C_2H_6}$ was defined as the ratio between the number of moles of C_2H_6 to the total number of moles of hydrocarbons. Based on the composition set by ϕ_M, the new composition simply replaced $x_{C_2H_6}$ moles of CH_4 with C_2H_6, for every mole of CH_4, without modifying the quantity of air. Hence, the total equivalence ratio (ϕ_{HC}) was higher for any given ϕ_M when C_2H_6 is present.

H_2 was added in some engine experiments to simulate the recycle of unused H_2, after separation from the tail gas of a methanol synthesis reactor. Steady-state flow models of the entire gas-to-liquids process for methanol synthesis indicated that the engine input can be 5 mol% H_2. This model assumed 60% conversion of the syngas to methanol in a two-stage synthesis step. Note that recycling of the neat tail gas into the methanol synthesis reactor is not feasible because of the nitrogen content, so an H_2/N_2 separator would be needed to accomplish the H_2 recycle. The intake composition including both C_2H_6 and H_2 is shown in Eq. 6, and ϕ_{HC} can be computed using Eq. 7, where H_2 is not considered to be a fuel. Note that $\phi_{HC} = \phi_M$ when $x_{C_2H_6} = 0$, as expected.

$$(1 - x_{C_2H_6})\, CH_4 + x_{C_2H_6}\, C_2H_6 + \frac{2}{\phi_M}\,(O_2 + 3.773\, N_2) + \frac{x_{H_2}}{1 - x_{H_2}}\left[1 + \frac{2}{\phi_M} 4.773\right] H_2 \qquad (6)$$

$$\phi_{HC} = \frac{\phi_M}{2}\left[2(1 - x_{C_2H_6}) + \frac{7}{2} x_{C_2H_6}\right] \qquad (7)$$

The conversion efficiency of CH_4 and C_2H_6, and carbon balance were calculated by normalizing to the N_2 (which is inert in the process, to very high accuracy) throughput. No NO_x gases were detected by the GC. These conversions were calculated by comparing mole throughput in exhaust mixtures to those in the intake, and are expressed as CH_4 conversion efficiency X_{CH_4} (Eq. 8), C_2H_6 conversion efficiency $X_{C_2H_6}$ (Eq. 9) and the moles of carbon in the exhaust relative to moles of carbon in the intake C_{Bal} (Eq. 10). The intake mole fractions are determined from the intake composition expressed in Eq. 6.

$$X_{CH_4} = 1 - \frac{x_{CH_4,exh}}{x_{CH_4,in}} \cdot \frac{x_{N_2,in}}{x_{N_2,exh}} \qquad (8)$$

$$X_{C_2H_6} = 1 - \frac{x_{C_2H_6,exh}}{x_{C_2H_6,in}} \cdot \frac{x_{N_2,in}}{x_{N_2,exh}} \qquad (9)$$

$$C_{Bal} = \frac{2x_{C_2H_6,exh} + x_{CO,exh} + x_{CO_2,exh} + x_{CH_4,exh}}{x_{CH_4,in} + 2x_{C_2H_6,in}} \cdot \frac{x_{N_2,in}}{x_{N_2,exh}} \qquad (10)$$

To provide a measure of the net work performed by the test cylinder, the net indicated mean effective pressure ($nimep$) was defined as the net work (the integral of cylinder pressure with respect to cylinder volume across the whole cycle) per engine cycle $W_{c,i,net}$, divided by the cylinder displacement V_d (Eq. 11). This provided a relative measure of work output against different engines. The coefficient of variation (COV) of $nimep$, or COV_{nimep}, was used to quantify the variation in combustion performance from cycle to cycle. The COV_{nimep} is the standard deviation of $nimep$ ($\boldsymbol{\sigma_{nimep}}$) divided by the mean of $nimep$ ($\boldsymbol{nimep_{mean}}$) across 200 consecutive engine cycles (Eq. 12) [25].

$$nimep = \frac{W_{c,i,net}}{V_d} \qquad (11)$$

$$COV_{nimep} = \left[\frac{\sigma_{nimep}}{nimep_{mean}}\right]_{200\ cycles} \qquad (12)$$

Intake Temperature

Engine performance was compared for a range of elevated intake temperatures from 350 °C to 460 °C. Preheating was required to achieve robust combustion at high equivalence ratios (ϕ_M > 1.8) as the premixed laminar flame speed of CH_4 is known to increase with temperature. Premixed laminar flame speeds provide a way to compare the combustibility of different fuel/air mixtures. Laminar flame speed is also relevant for misfire, as the initial development of the combustion kernel during the sparking event is related to the laminar flame speed. Turbulence in the cylinder speeds up the combustion process, but the turbulent flame speed also scales with the laminar flame speed. [25,26] Karim et al reported an increase in the rich mixture operating limit when increasing intake charge temperature from 25 °C to 130 °C. [19]

At ambient initial temperature and pressure, the maximum laminar flame speed of CH_4 is 35 cm/s at $\phi_M \sim 1.1$. At equivalence ratios above 1.5, this value drops below 10 cm/s. [27] In order to improve combustion and overall engine performance at ϕ_M > 1.8, higher flame speeds are possible at elevated temperatures by pre-heating intake mixtures. For example, at methane-air equivalence ratios of 1.4, the flame speed of a mixture with initial temperature of 34 °C was computed to be 22 cm/s, while that with a temperature of 342 °C had a flame speed of 88 cm/s. [28]

Figure 2 shows the H_2 to CO ratio as a function of intake temperature, for equivalence ratios between 1.8 and 2.0. Intake mixtures were heated to between 350 °C and 460 °C to investigate the effect of higher temperatures on combustion performance in the engine cylinder. Baseline spark timing of 30° BTDC was used, and intake pressure was maintained at 1.1 bar. At ϕ_M of 1.8, 1.9 and 2.0, X_{CH_4} was 90% across the test range, suggesting that intake temperatures > 350 °C are sufficient for robust spark ignition and flame propagation across the cylinder. Though there appeared to be a small increase in conversion efficiency at higher temperatures, this amount was not significant. The H_2 to CO ratio in the exhaust gases range increased with ϕ_M. This is due to the larger amount of hydrogen available at higher equivalence ratios from CH_4. Tests performed at temperatures below 350 °C resulted in significant misfire, and therefore are not shown here.

Figure 3(a) shows the peak pressure as a function of intake temperature. Peak cylinder pressures were flat across the temperature range tested, but were higher for lower equivalence ratios, from 60 bar for ϕ_M = 2.0, to 75 bar for ϕ_M = 1.8. Peak pressure is a function of heat released before top-dead-center (TDC), and the trend shown here is consistent with decreasing equivalence ratio where the quantity of O_2 is higher. At the same time, the average $nimep$ ($nimep_{mean}$) decreased slightly with respect to temperature, and was independent of equivalence ratio for a given intake temperature. The total work is a function of the total chemical energy released during combustion, which should tend to decrease with lower charge densities. With a 16% increase in temperature (calculated in Kelvin) and therefore decrease in density by the same fraction, $nimep_{mean}$ dropped from 400 kPa to 350 kPa across the temperature range (13 % decrease). However, since the objective is not to maximize work output, this is not a concern. In other tests where intake temperature was held constant, > 450 °C was maintained as a precaution to ensure that the maximum flame speed was obtained given

the limitations on the heating apparatus. In practice, this may not be necessary since the engine's performance with > 350 °C intake charge temperature appeared to be sufficient.

Spark Timing

Figure 4(a) shows $nimep_{mean}$ as a function of spark timing at $\phi_M = 2.0$, intake temperature of 450 °C, and intake pressure of 1.1 bar. Advancing spark timing, from 30° to 45° before top-dead-center (BTDC) piston position increased peak pressure, but produced significantly lower combustion stability (lower COV_{nimep}), lower values of $nimep_{mean}$, and lower CH_4 conversion efficiency (Fig. 5). The figures in 4(b) show the in-cylinder pressure as a function of crank angle, for 200 consecutive cycles and a corresponding histogram of the peak pressure for those 200 cycles. Combustion stability was quantified by COV_{nimep}. Therefore, in operating regimes where the engine alternated between periods of combustion and large periods of misfire (where combustion failed to occur entirely), the average net work output was small and the standard deviation large, resulting in very large values of COV_{nimep}. At spark timing of 45° BTDC a substantial number of engine cycles were misfires (large frequency of engine cycles with peak pressure of 30 bar in Fig. 4(b,1R), corresponding to misfire). In contrast, with 30° BTDC spark timing, the histogram frequency of 30 bar peak pressure was small as shown in Figure 4(b,4R).

Spark timing advancement led to ignition occurring increasingly before top-dead-center (TDC), when the in-cylinder pressure and temperature at sparking were both lower. There are two competing mechanisms. First, lower mixture pressure and temperature at sparking led to lower flame speeds and combustibility of the gas; as a result there was a higher incidence of misfire with increasingly advanced spark timing as shown in Figure 4(b,1L/R). However, earlier spark events allowed the gas more time to react, and therefore more heat to be released if combustion were to occur at all. This explains the higher peak pressures achieved during successful combustion cycles (Fig. 4(b,1R), maximum peak pressures were 80 bar, while in Fig. 4(b,4R), maximum peak pressures were 70 bar), and the slight gain in H_2:CO ratio > 1.4 with advanced timing (Fig. 5). The net result is that the most advanced timing led to higher maximum peak pressures, but significant misfire led to low $nimep_{mean}$ (~ 200 kPa), poor CH_4 conversion (~ 60 %), and high values of COV_{nimep} (> 100 %), in comparison to $nimep_{mean}$ ~ 350 kPa, CH_4 conversion ~ 90 % and COV_{nimep} < 20 % with 30° BTDC timing.

Overall, a delay in spark timing led to a slight decrease in syngas quality (lower H_2 to CO ratio) as it led to lower overall peak pressures, lower peak cylinder temperatures [25], and therefore an equilibrium in the water-gas shift reaction that favored CO production. However, this delay also led to a significant improvement in combustion stability, and therefore was preferable for syngas production due to smoother operation. For the remainder of the paper, 30° BTDC spark timing was used.

Equivalence Ratio

The engine demonstrated robust combustion with COV_{nimep} < 20% at ϕ_M= 2.0, in the absence of hydrogen or ethane, at inlet temperature and pressure 450 °C and 1.1 bar, and

spark timing of 30° BTDC. This defined the "borderline" condition without chemical assistance from H_2 or C_2H_6, both of which increased flame speed. At an equivalence ratio ϕ_M = 2.1 (Fig. 6 (3L,R)), misfire occurred frequently enough to reduce combustion stability and increase COV_{nimep} up to 30 % (Fig. 11), and reduce X_{CH_4} below 90% (Fig. 9). At the "borderline" condition of ϕ_M = 2.0, the engine could still operate reliably without H_2 recycle, though at the expense of relatively low H_2 to CO ratio of 1.3. Note that since results showing C_2H_6 addition are also included in this section, the presence of C_2H_6 is noted in the plot legends.

Figure 7 shows the peak pressure as a function of equivalence ratio, showing the results both with and without hydrogen and ethane addition. Peak pressure tended to fall with increasing equivalence ratios, from ϕ_{HC} = 1.8 to 2.8, at the same spark timing of 30° BTDC. The peak pressure was reduced somewhat by the strong presence of misfire, so only conditions with COV_{nimep} < 35% are shown here. The peak pressure achieved in the combustion chamber depends on the cumulative heat released before TDC. For the same spark timing, richer mixtures would release less heat due to the lack of O_2 to perform complete combustion (which is more exothermic than partial oxidation, as shown in Eq. 1 and 2). Naturally, more partial oxidation occurred at higher values of ϕ_{HC}, and hence smaller peak pressures were developed at these conditions. The relative advantage in heat release is seen at $\phi_{HC} = 2.2$, where H_2 addition increased the average peak pressure from 47 bar to 55 bar. At $\phi_{HC} \geq 2.4$ and without H_2, combustion was poor and results are not shown. However, the benefit of C_2H_6 is compared at these equivalence ratios, where heat release was higher due to the increase in heating value of the mixture when 10% by volume of CH_4 was effectively replaced with C_2H_6. The heating value per mole of fuel of C_2H_6 is almost double that of CH_4 (the lower heating values are 1560 kJ/mol and 890 kJ/mol respectively). For example, at $\phi_{HC} = 2.8$, H_2 addition without C_2H_6 yielded a peak pressure of only 37 bar (the motoring trace peaked at 30 bar). The addition of C_2H_6 increased the peak pressure significantly to 47 bar, which corresponded to combustion at $\phi_{HC} = 2.2$ with neither H_2 nor C_2H_6. However, the benefit of C_2H_6 on heat release (and therefore peak pressure) at high equivalence ratios must be matched with the appropriate composition in exhaust gases, and this is where we must weigh the chemical inefficiencies at the extreme operating regimes.

Figure 8 shows the H_2 to CO ratio for the same data as Figure 7. As expected, increasing the equivalence ratio, even in the absence of hydrogen, increased the H_2 to CO ratio. However, there was a much larger impact when H_2 or C_2H_6 were added. The presence of either increased the H_2 to CO ratio by about 0.3 (from 1.3 to 1.6), and extended the maximum operating equivalence ratio further. It should be noted, however, that the addition of ethane did not substantially affect the H_2 to CO ratio, over that with just hydrogen addition.

Figure 9 shows the conversion efficiency of the hydrocarbons for the same data as shown in Figures 7-8. The downside of operating at increased equivalence ratio $\phi_{HC} \geq 2.4$ was reduced conversion. The conversion of CH_4 and C_2H_6 both fell below 90% at these equivalence ratios, and as low as 65% for CH_4 at $\phi_{HC} = 2.8$. Given these deficiencies, the upside of operating at these rich mixtures were twofold. First, the addition of H_2 and C_2H_6 led to low COV_{nimep} < 5% as a result of stable combustion. Figure 10 shows

COV_{nimep} for the same data as Figures 7-9. The flame speed of the rich mixtures tested at $\phi_{HC} \geq 2.4$ were simulated in Cantera and found to be < 10 cm/s. While this is low, it apparently does not lead to large variability. That is to say, not all of the CH_4 reacted, but its conversion was stable from cycle-to-cycle. Fig. 11 demonstrates the effect of H_2 and C_2H_6 on combustion variability, for the same data in Figures 7-10, where the histogram of peak pressures fell within a band 5-8 bar wide when those gases were added. Second, high equivalence ratios $\phi_{HC} \geq 2.4$ were needed to produce exhaust mixtures with H_2 to CO ratios close to 2.0, which is desirable for liquids synthesis. There did not appear to be a benefit to the H_2 to CO ratio by replacing 10% of the CH_4 with C_2H_6, though the effect is not detrimental. In fact, the conversion of C_2H_6 did not fall below 80% even in the richest conditions (Fig. 9), though there appears to be a downward trend in conversion similar to that for CH_4.

Ultimately, a compromise must be made between the absolute quantity of CH_4 converted, and the H_2 to CO ratio that can be achieved in the exhaust gas. The volumetric flow rate of CH_4 at standard conditions (25 °C, 1 atm) that was inducted into the engine, and that was converted ($\dot{V}^{\circ}_{CH_4} \cdot X_{CH_4}$), is shown in Figure 12, using the conversion efficiencies shown in Figure 9. This demonstrates that the highest flow rates occur for cases without H_2 and C_2H_6, which of course were both added in place of CH_4, hence reducing the overall flow rate of CH_4. More importantly, $\phi_{HC} \geq 2.4$ showed a downward trend in $\dot{V}^{\circ}_{CH_4} \cdot X_{CH_4}$, likely due to the decrease in methane conversion efficiency due to extremely rich operation (Figure 9). It appears that the optimum equivalence ratio is ϕ_{HC} = 2.2 with H_2 recycle, where the H_2 to CO ratio was ~ 1.8, and where combustion did not suffer from significant conversion inefficiency.

Ethane Concentration

The effect of C_2H_6 on engine reforming capability was studied by varying its concentration relative to CH_4. In the experiment, we replace methane by ethane on a 1-to-1 basis, by 5% increments up to 20%. That is to say, we kept the total number of moles of fuel the same, and steadily increase the fraction occupied by C_2H_6. In the figures described in this section, ϕ_M is the value defined in Eq. 6, where a fraction $x_{C_2H_6}$ of CH_4 was replaced with C_2H_6. Figure 13 shows that at constant values of ϕ_M, the H_2 to CO ratio in the exhaust did not vary significantly, up to $x_{C_2H_6} = 20\%$. The ideal partial oxidation of C_2H_6 produces an H_2 to CO ratio of 1.5, which may explain this mild relationship. The large difference in H_2 to CO ratio between $\phi_M = 2.0$ and 2.4 is expected, and this was demonstrated earlier in Figure 8, which showed that leaner mixtures achieved lower H_2 to CO ratios than richer ones.

Figure 14 shows the CH_4 conversion as a function of $x_{C_2H_6}$, for the same conditions as Figure 13. The practical effect of increasing $x_{C_2H_6}$ while keeping the total number of moles of fuel constant is that the overall hydrocarbon-air equivalence ratio increases ($\phi_{HC} > \phi_M$), leading to decreased CH_4 conversion due to poorer reactivity, e.g. 65% conversion with $x_{C_2H_6}$ = 20%, compared to 75% conversion with $x_{C_2H_6}$ = 0%. The decrease in CH_4 conversion was not seen when ϕ_M = 2.0, where CH_4 conversion values did not fall below 87% regardless of the value of $x_{C_2H_6}$ (up to 20%). At these lower

equivalence ratios, the mixture was reactive enough to burn to close to completion in the given cycle time.

Figures 15 and 16 show the peak pressure and the COV_{nimep} for the same conditions as Figures 13 and 14. Increasing the concentration of C_2H_6 resulted in higher peak pressures with consistently low values of COV_{nimep}. For $x_{C_2H_6}$ > 10% however, the peak pressure was insensitive to $x_{C_2H_6}$. It is likely that low flame speeds coupled with decreasing CH_4 conversion was the cause of this plateau in peak pressure.

Soot Concentration in Exhaust Gases

Figure 17 shows exhaust soot concentrations, measured gravimetrically across a range of hydrocarbon-air equivalence ratios, with and without H_2 and C_2H_6 addition. The soot concentrations at $\phi_{HC} \geq 2.4$ were found to be on the same order of magnitude as maximum concentrations found in a swirl-chamber IDI diesel engine, [29] and ranged from 1-3 mg/L. The increase in the value of ϕ_{HC} led to a steep rise in soot output, at approximately a rate of 22.5 mg/L for every unit increase in ϕ_{HC} above a value of $\phi_{HC} = 2.4$. This rise is expected to plateau as the flame speed of the mixture would be too low above a certain value of ϕ_{HC}. These large concentrations of soot would be detrimental to catalytic systems downstream of the engine. Therefore, either a particulate filter would have to be installed and frequently regenerated, or the engine would have to be operated at a lower equivalence ratio to prevent high soot output from occurring. The increase in soot production with equivalence ratio is supported by the reduction in carbon balance through the engine (Figure 18). Overall carbon balance, for the cases in Figures 7-10, is shown in Figure 18. The carbon balance is performed with respect to the dry exhaust gases sampled by the gas chromatograph, relative to the intake mixture composition. A reduction in carbon balance at high values of ϕ_{HC} is likely a result of high soot production at those conditions.

According to EPA Title 40: Protection of Environment PART 1039 Subpart B, which regulates particulate matter (PM) emissions from new and in-use nonroad compression-ignition engines, the maximum allowable PM emissions is 0.4 g /kWh, [30] or 0.5 mg/L, for a 0.5 L, 19 kW diesel engine operating at 1000 rpm. The values obtained in experiment are up to 9 times higher than this standard at $\phi_{HC} \geq 2.2$. However, federal regulations are not fair metrics for evaluation for three reasons. First, the engine is intentionally run with low combustion efficiency and high equivalence ratio in order to obtain the desired chemical composition at exhaust. High soot production under these extreme conditions is not surprising. Second, regulations are with respect to tailpipe emissions, and therefore do not cite the intermediate values that occur in the exhaust manifold. Regulations are satisfied with the help of diesel particulate filters and catalytic converters, neither of which were used in these tests. Lastly, in practice, the engine will be in line with a synthesis reactor and its emissions will not be passed to the atmosphere. There will likely be a cleanup step to manage and remove any soot produced. In the future, liquid water injecting in the cylinder will be tested to determine its effect on soot formation at high equivalence ratios.

Soot Propensity Calculations

To better understand soot formation in the engine, we simulated a premixed rich flame using the USC Mech II chemistry model. Benzene – a precursor to soot – was used to qualitatively compare sooting trends as a function of fuel equivalence ratio. Flat, premixed laminar flame simulations were conducted for the conditions in Figure 16 for unburned gas temperatures of 750 K and at a pressure of 9 atm (an estimation of the physical state of the unburned fuel mixture at the moment of ignition). Peak benzene concentrations were used to infer the sooting propensity of fuel rich mixtures relative to ϕ_{HC} = 2. The relative quantities of benzene formation for different hydrocarbon-air equivalence ratios are shown in Table 5. A qualitative trend can be seen for this laminar flame that also predicts the monotonic increase in soot production with increasing equivalence ratio. In reality, soot production was accelerated due to turbulence in the engine cylinder. [31]

Table 5. The relative quantity of benzene that was computed at various hydrocarbon-air equivalence ratios (ϕ_{HC}).

$\boldsymbol{\phi_{HC}}$	**Relative Benzene Formation Normalized to $\boldsymbol{\phi_{HC}}$ = 2.0**
2.00	1.00
2.20	1.71
2.37	2.00
2.40	2.24
2.58	2.38
2.80	2.58

Conclusion:

We have demonstrated reliable operation of an engine reformer running on atmospheric air for the production of syngas. We have shown that intake temperatures > 350 °C are sufficient to reach stable combustion with room air, at methane-air equivalence ratios ϕ_M up to 2.0. Spark timing at 30 ° BTDC provided significant improvements to combustion stability when compared to more advanced timing. A hydrocarbon-air equivalence ratio ϕ_{HC} of 2.2 with 5% H_2 recycle from downstream processes provided an acceptable balance of high H_2 to CO ratio ~ 1.8, high CH_4 conversion efficiency ~ 85%, and low exhaust soot concentration ~ 0.18 mg/L. Lower than this ratio led to a dramatic reduction in H_2 to CO ratio, which would have required significant water-gas shift to boost this ratio closer to 2.0. Higher than this ratio led to a significant reduction in CH_4 conversion efficiencies, and large quantities of soot production. These results provide operating guidelines for the selection of a larger engine reformer to be used in a demonstration natural-gas-to-methanol system in the near future. With the lower cost economics brought about by the engine reformer, compact gas-to-liquids system can now reach significantly smaller scale than was possible in the past. This may finally allow previously untapped associated gas sites to be utilized in a cost-competitive way.

Acknowledgements:

We would like to thank ARPA-e, the MIT Energy Initiative, and Tata Center for Technology and Design at MIT for their generous support. We would also like to thank Kyle Merical and Paul Yelvington from Mainstream Engineering, John Carpenter at the Research Triangle Institute, Klaus Lackner at Arizona State University, and Josh Browne at Columbia University for their thoughtful feedback.

Nomenclature

atm	Atmospheres of pressure
C_{Bal}	Carbon balance; ratio of moles of C in dry exhaust to moles of C in intake
COV_{nimep}	Coefficient of variation of net indicated mean effective pressure (%)
BDC	Bottom-dead-center
boe/d	Barrels of oil equivalent per day
CAD	Crank angle degree (°)
GTL	Gas-to-liquids
ΔH°_{298}	Reaction enthalpy at 298 K
kJ/mol	Kilojoules per mole
$\dot{m}_{engine}$	Mass flow rate at engine intake (g/s)
M_{mix}	Molar mass of intake mixture (g/mol)
mmscfd	Million standard cubic feet per day
MS5A	CP-Molsieve 5A
MT/yr	Metric tons per year
N	Engine speed (rev/min)
$nimep$	Net indicated mean effective pressure (kPa)
$nimep_{mean}$	Average net indicated mean effective pressure (kPa)
NO_x	Nitrogen oxides
$p_{cyl,pk}$	Average peak cylinder pressure (bar)
ϕ_{HC}	Total hydrocarbon-air equivalence ratio
ϕ_M	Total hydrocarbon-air equivalence ratio, assuming all moles of fuel are CH_4
p_i	Intake pressure
PPU	PoraPLOT U
PSA	Pressure swing adsorption
PSIA	Pounds per square inch, absolute
R	Universal gas constant $\left(\frac{L\ kPa}{K\ mol}\right)$
Scfh	Cubic feet per hour at standard conditions (25 °C, 14.7 PSIA)
σ_{nimep}	Standard deviation of net indicated mean effective pressure (kPa)
SLPM	Liters per minute at standard conditions (25 °C, 14.7 PSIA)
T_i	Intake mixture temperature (°C); when used in $\dot{m}_{engine}$ this is in (K)
$\dot{V}^{\circ}_{CH_4}$	Intake volumetric flow rate of CH_4 at 25 °C, 1 atm (standard) conditions
V_d	Engine displacement volume (L)
VDC	Volts, direct current
$W_{c,i,net}$	Net indicated work output per cycle
$x_{C_2H_6}$	Mole fraction of C_2H_6 in hydrocarbon (C_2H_6 and CH_4) fuel
$X_{C_2H_6}$	Conversion efficiency of C_2H_6
X_{CH_4}	Conversion efficiency of CH_4
x_{H_2}	Mole fraction of H_2 in intake mixture
$x_{i,exh}$	Mole fraction of compound i in dry exhaust
$x_{i,in}$	Mole fraction of compound i in intake mixture

Figures

List of Figure Captions

1. The engine reformer may be coupled with a liquids synthesis reactor to produce methanol from natural gas.
2. H_2 to CO ratio in engine exhaust across three methane-air equivalence ratios (ϕ_M = 1.8, 1.9, 2.0), from 360 °C to 460 °C intake temperature. No H_2 or C_2H_6 was added to the intake mixture, which was maintained at 1.1 bar. Spark ignition occurred at 30° BTDC. Each point corresponds to one sample collected on the gas chromatograph.
3. (a) Average peak cylinder pressure ($p_{cyl,pk}$) and (b) average net indicated mean effective pressure ($nimep_{mean}$), from 360 °C to 460 °C intake temperature. No H_2 or C_2H_6 was added to the intake mixture, which was maintained at 1.1 bar. Spark ignition occurred at 30° BTDC. Each point corresponds to the average across 200 consecutive engine cycles.
4. (a) $nimep_{mean}$ and coefficient of variation of $nimep$ (COV_{nimep}) with 30° to 45° BTDC spark timing advancement. Each point corresponds to the average across 200 consecutive engine cycles. (b) The corresponding (L) cylinder pressure traces for a subsection of compression and expansion strokes, and (R) histograms of peak cylinder pressure for those traces at (1) 45° BTDC, (2) 40° BTDC, (3) 35° BTDC and (4) 30° BTDC. Each pressure trace plot and histogram displays 200 consecutive engine cycles.
5. H_2 to CO ratio in exhaust gases, and CH_4 conversion efficiency (%) with 30° to 45° BTDC spark timing advancement. ϕ_M was held constant at 2.0, T_i at 450 °C, and p_i at 1.1 bar. Each point corresponds to one sample collected on the gas chromatograph.
6. (L) Cylinder pressure traces for subsection of compression and expansion strokes, and (R) histograms of peak cylinder pressure for those cycles. (1) ϕ_M = 1.9, (2) ϕ_M = 2.0, (3) ϕ_M = 2.1. T_i and p_i were both held constant at 450 °C and 1.1 bar respectively. Each pressure trace plot and histogram corresponds to 200 consecutive engine cycles.
7. Average peak cylinder pressure for hydrocarbon-air equivalence ratios ϕ_{HC} from 1.8 to 2.8. Contrasts effect of H_2 and C_2H_6 on peak cylinder pressure. Each point corresponds to the average of 200 consecutive engine cycles.
8. H_2 to CO ratios for hydrocarbon-air equivalence ratios ϕ_{HC} from 1.8 to 2.8. Contrasts effect of H_2 and C_2H_6 on H_2 to CO ratio. Each point corresponds to one sample collected on the gas chromatograph.
9. Conversion efficiency for CH_4 and C_2H_6 (noted on legend) for hydrocarbon-air equivalence ratios ϕ_{HC} from 1.8 to 2.8. Contrasts effect of H_2 and C_2H_6 on conversion efficiency of the two fuels. Each point corresponds to one sample collected on the gas chromatograph.
10. Coefficient of variation of $nimep$ (COV_{nimep}) for hydrocarbon-air equivalence ratios ϕ_{HC} from 1.8 to 2.8. Demonstrates improvement that H_2 and C_2H_6 have on COV. Each point corresponds to the average of 200 consecutive engine cycles.

11. (L) Cylinder pressure traces for subsection of compression and expansion strokes, and (R) histograms of peak cylinder pressure for those cycles. (1) ϕ_{HC} = 2.2, x_{H_2} = 0%, $x_{C_2H_6}$ = 0%, T_i = 450 °C, p_i = 1.1 bar, (b) ϕ_M = 2.2, x_{H_2} = 5%, $x_{C_2H_6}$ = 0%, T_i = 480 °C, p_i = 1.1 bar, (c) ϕ_{HC} = 2.4, x_{H_2} = 5%, $x_{C_2H_6}$ = 10%, T_i = 480 °C, p_i = 1.1 bar. Each pressure trace plot and histogram corresponds to 200 consecutive engine cycles.
12. Standard volumetric flow rate of CH_4 at the intake that was converted in the engine ($\dot{V}^{\circ}_{CH_4} \cdot X_{CH_4}$), based on conversion efficiency data in Figure 9. Each point corresponds to one sample collected on the gas chromatograph.
13. H_2 to CO ratio for different concentrations of C_2H_6 in CH_4 ($x_{C_2H_6}$, expressed as a percentage) from 0% to 20%. Comparison shown for ϕ_M = 2.0 (x_{H_2} = 0%) and 2.4 (x_{H_2} = 5%) with different values of $x_{C_2H_6}$. Note: the value of ϕ_{HC} is not the same at different $x_{C_2H_6}$. Each point corresponds to an average of 200 consecutive engine cycles.
14. CH_4 conversion efficiency (X_{CH_4}), expressed as a percentage, for different concentrations of C_2H_6 in CH_4 ($x_{C_2H_6}$, expressed as a percentage) from 0% to 20%. Comparison shown for ϕ_M = 2.0 (x_{H_2} = 0%) and 2.4 (x_{H_2} = 5%) with different values of $x_{C_2H_6}$. Each point corresponds to an average of 200 consecutive engine cycles.
15. Average peak cylinder pressure ($p_{cyl,pk}$) for different concentrations of C_2H_6 in CH_4 ($x_{C_2H_6}$, expressed as a percentage) from 0% to 20%. Comparison shown for ϕ_M = 2.0 (x_{H_2} = 0%) and 2.4 (x_{H_2} = 5%) with different values of $x_{C_2H_6}$. Each point corresponds to an average of 200 consecutive engine cycles.
16. Coefficient of variation of *nimep* (COV_{nimep}) for different concentrations of C_2H_6 in CH_4 ($x_{C_2H_6}$, expressed as a percentage) from 0% to 20%. Comparison shown for ϕ_M = 2.0 (x_{H_2} = 0%) and 2.4 (x_{H_2} = 5%) with different values of $x_{C_2H_6}$. Each point corresponds to an average of 200 consecutive engine cycles.
17. Soot concentration in exhaust gases, measured gravimetrically, at hydrocarbon-air equivalence ratios ϕ_{HC} = 2.0 to 2.8, contrasting the effects of H_2 and C_2H_6.
18. Carbon balance through engine, at hydrocarbon-air equivalence ratios ϕ_{HC} = 1.8 to 2.8.

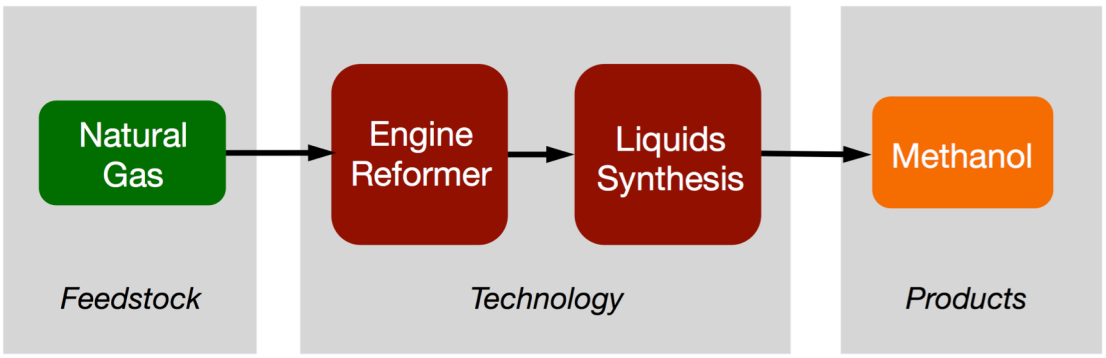

Figure 1. The engine reformer may be coupled with a liquids synthesis reactor to produce methanol from natural gas.

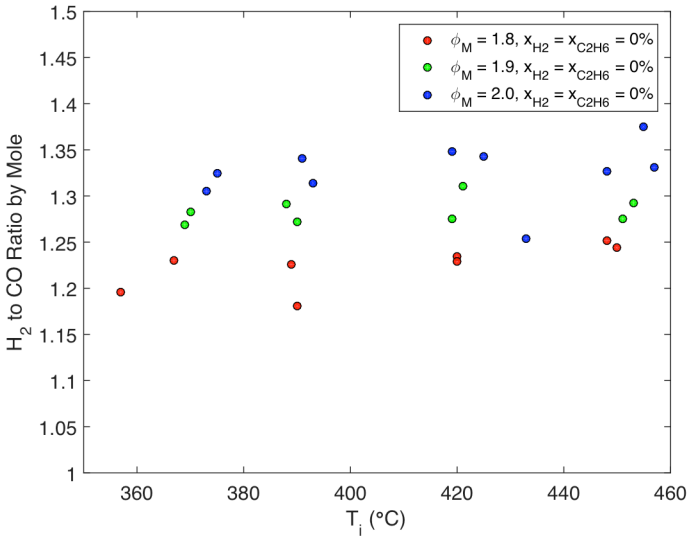

Figure 2. H_2 to CO ratio in engine exhaust across three methane-air equivalence ratios (ϕ_M = 1.8, 1.9, 2.0), from 360 °C to 460 °C intake temperature. No H_2 or C_2H_6 was added to the intake mixture, which was maintained at 1.1 bar. Spark ignition occurred at 30° BTDC. Each point corresponds to one sample collected on the gas chromatograph.

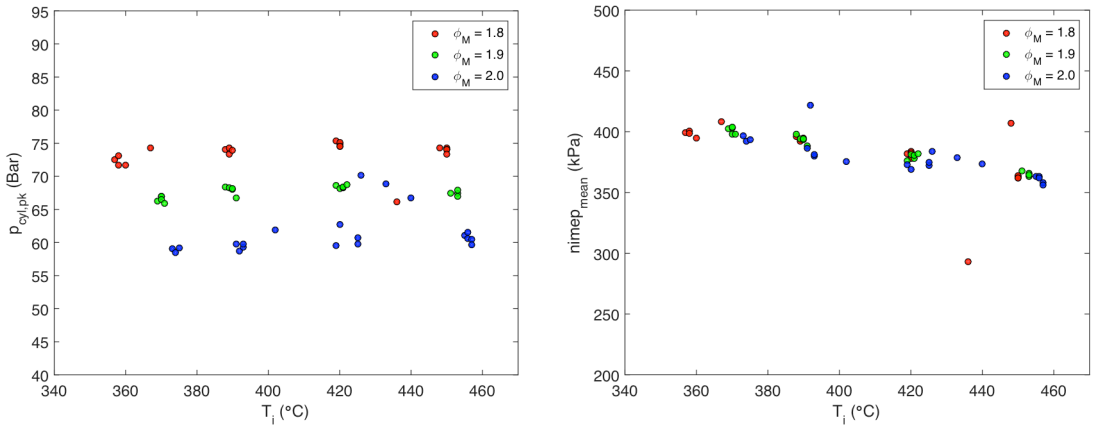

(a) **(b)**

Figure 3. (a) Average peak cylinder pressure ($p_{cyl,pk}$) and (b) average net indicated mean effective pressure ($nimep_{mean}$), from 360 °C to 460 °C intake temperature. No H_2 or C_2H_6 was added to the intake mixture, which was maintained at 1.1 bar. Spark ignition occurred at 30° BTDC. Each point corresponds to the average across 200 consecutive engine cycles.

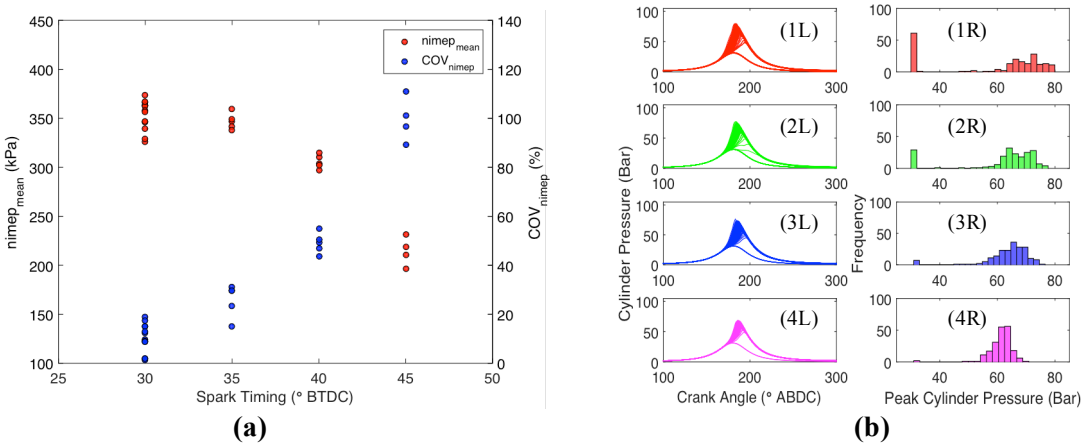

Figure 4. (a) $nimep_{mean}$ and coefficient of variation of $nimep$ (COV_{nimep}) with 30° to 45° BTDC spark timing advancement. Each point corresponds to the average across 200 consecutive engine cycles. (b) The corresponding (L) cylinder pressure traces for a subsection of compression and expansion strokes, and (R) histograms of peak cylinder pressure for those traces at (1) 45° BTDC, (2) 40° BTDC, (3) 35° BTDC and (4) 30° BTDC. Each pressure trace plot and histogram displays 200 consecutive engine cycles.

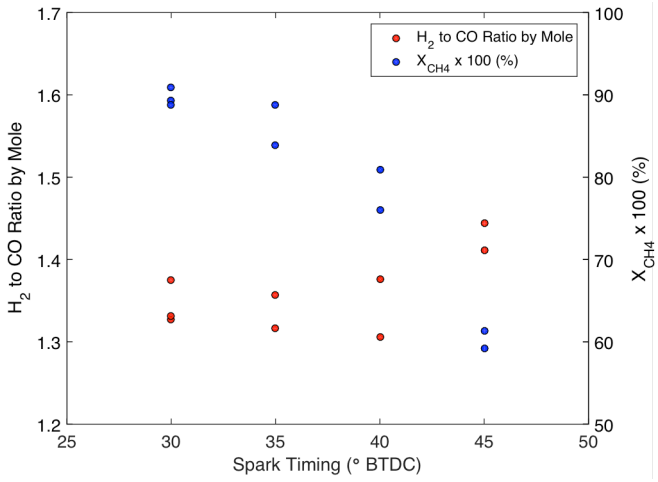

Figure 5. H_2 to CO ratio in exhaust gases, and CH_4 conversion efficiency (%) with 30° to 45° BTDC spark timing advancement. ϕ_M was held constant at 2.0, T_i at 450 °C, and p_i at 1.1 bar. Each point corresponds to one sample collected on the gas chromatograph.

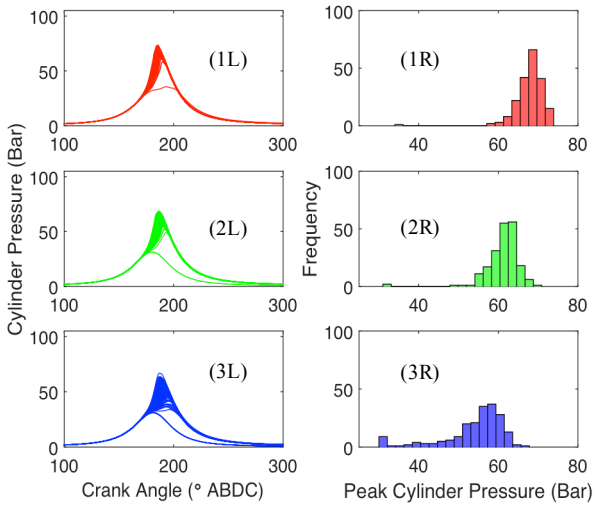

Figure 6. (L) Cylinder pressure traces for subsection of compression and expansion strokes, and (R) histograms of peak cylinder pressure for those cycles. (1) ϕ_M = 1.9, (2) ϕ_M = 2.0, (3) ϕ_M = 2.1. T_i and p_i were both held constant at 450 °C and 1.1 bar respectively. Each pressure trace plot and histogram corresponds to 200 consecutive engine cycles.

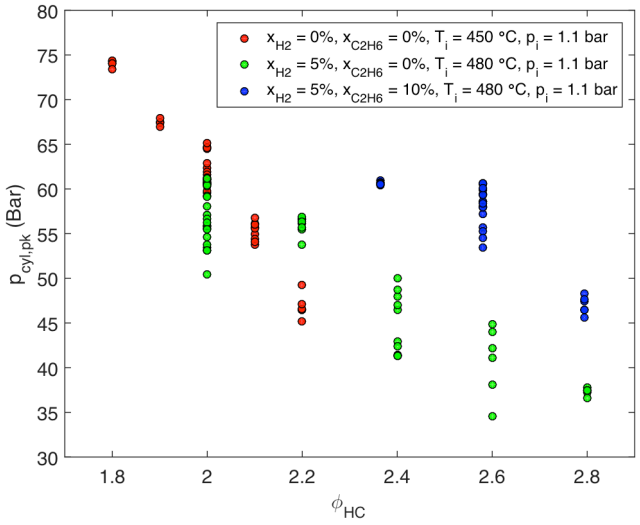

Figure 7. Average peak cylinder pressure for hydrocarbon-air equivalence ratios ϕ_{HC} from 1.8 to 2.8. Contrasts effect of H_2 and C_2H_6 on peak cylinder pressure. Each point corresponds to the average of 200 consecutive engine cycles.

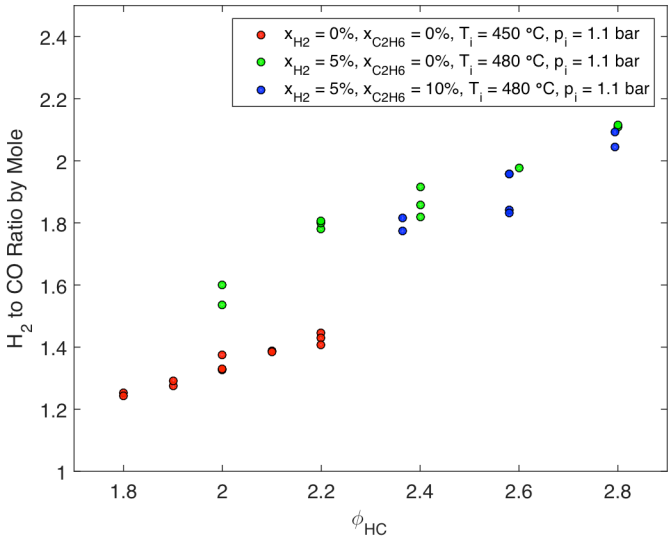

Figure 8. H_2 to CO ratios for hydrocarbon-air equivalence ratios ϕ_{HC} from 1.8 to 2.8. Contrasts effect of H_2 and C_2H_6 on H_2 to CO ratio. Each point corresponds to one sample collected on the gas chromatograph.

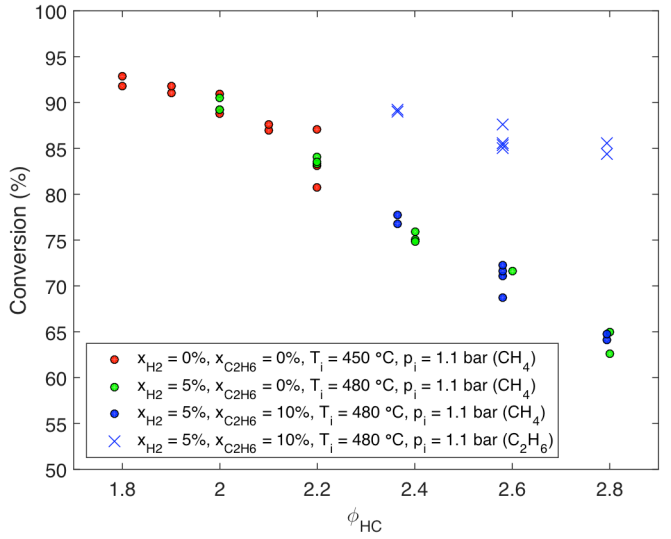

Figure 9. Conversion efficiency for CH_4 and C_2H_6 (noted on legend) for hydrocarbon-air equivalence ratios ϕ_{HC} from 1.8 to 2.8. Contrasts effect of H_2 and C_2H_6 on conversion efficiency of the two fuels. Each point corresponds to one sample collected on the gas chromatograph.

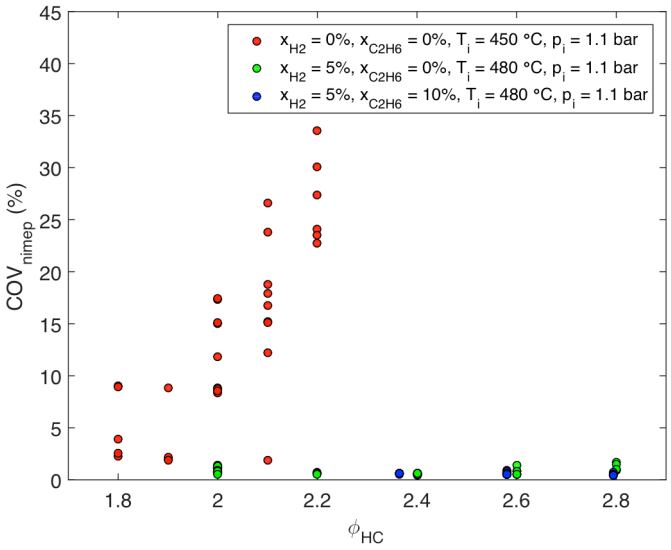

Figure 10. Coefficient of variation of $nimep$ (COV_{nimep}) for hydrocarbon-air equivalence ratios ϕ_{HC} from 1.8 to 2.8. Demonstrates improvement that H_2 and C_2H_6 have on COV. Each point corresponds to the average of 200 consecutive engine cycles.

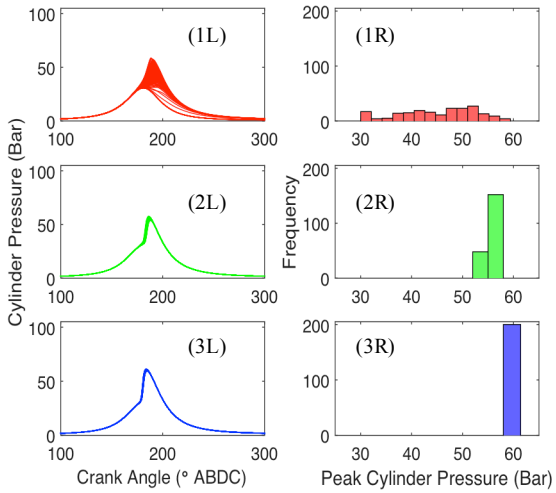

Figure 11. (L) Cylinder pressure traces for subsection of compression and expansion strokes, and (R) histograms of peak cylinder pressure for those cycles. (1) ϕ_{HC} = 2.2, x_{H_2} = 0%, $x_{C_2H_6}$ = 0%, T_i = 450 °C, p_i = 1.1 bar, (b) ϕ_M = 2.2, x_{H_2} = 5%, $x_{C_2H_6}$= 0%, T_i = 480 °C, p_i = 1.1 bar, (c) ϕ_{HC} = 2.4, x_{H_2} = 5%, $x_{C_2H_6}$ = 10%, T_i = 480 °C, p_i = 1.1 bar. Each pressure trace plot and histogram corresponds to 200 consecutive engine cycles.

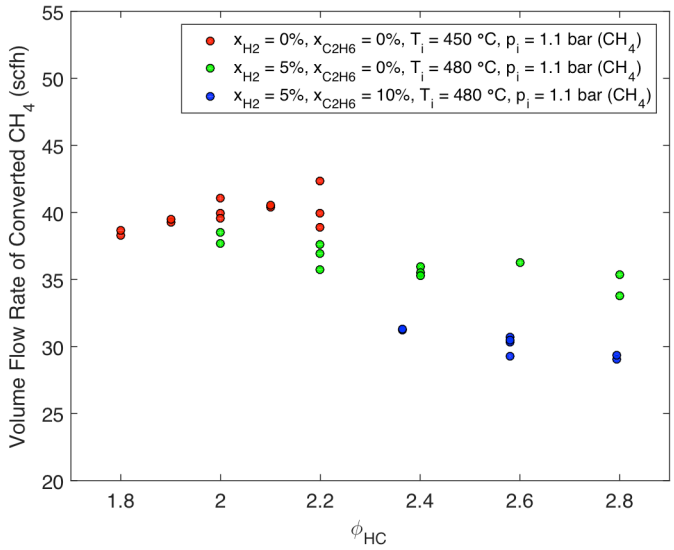

Figure 12. Standard volumetric flow rate of CH_4 at the intake that was converted in the engine ($\dot{V}^{\circ}_{CH_4} \cdot X_{CH_4}$), based on conversion efficiency data in Figure 9. Each point corresponds to one sample collected on the gas chromatograph.

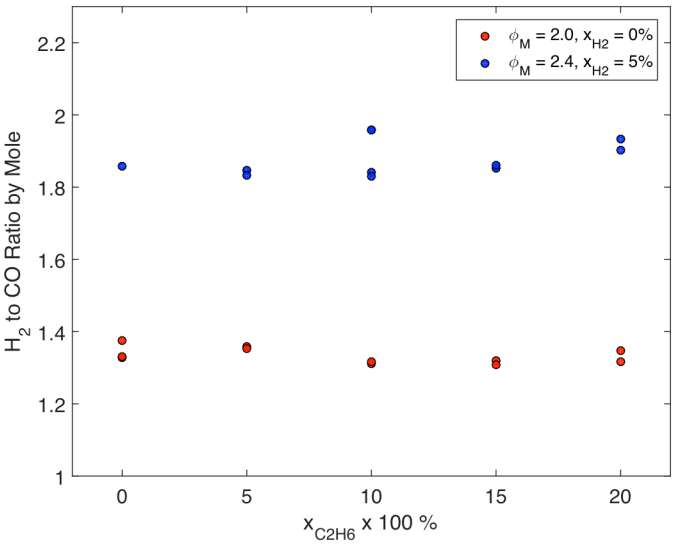

Figure 13. H_2 to CO ratio for different concentrations of C_2H_6 in CH_4 ($x_{C_2H_6}$, expressed as a percentage) from 0% to 20%. Comparison shown for $\phi_M = 2.0$ ($x_{H_2} = 0\%$) and 2.4 ($x_{H_2} = 5\%$) with different values of $x_{C_2H_6}$. Note: the value of ϕ_{HC} is not the same at different $x_{C_2H_6}$. Each point corresponds to an average of 200 consecutive engine cycles.

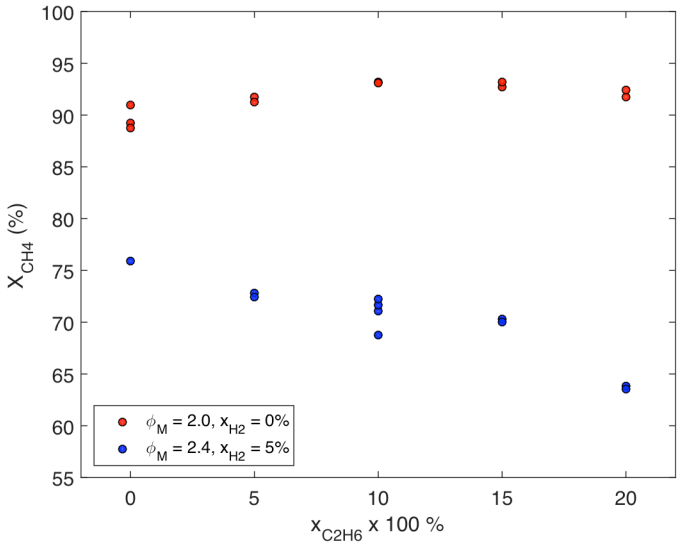

Figure 14. CH_4 conversion efficiency (X_{CH_4}), expressed as a percentage, for different concentrations of C_2H_6 in CH_4 ($x_{C_2H_6}$, expressed as a percentage) from 0% to 20%. Comparison shown for $\phi_M = 2.0$ ($x_{H_2} = 0\%$) and 2.4 ($x_{H_2} = 5\%$) with different values of $x_{C_2H_6}$. Each point corresponds to an average of 200 consecutive engine cycles.

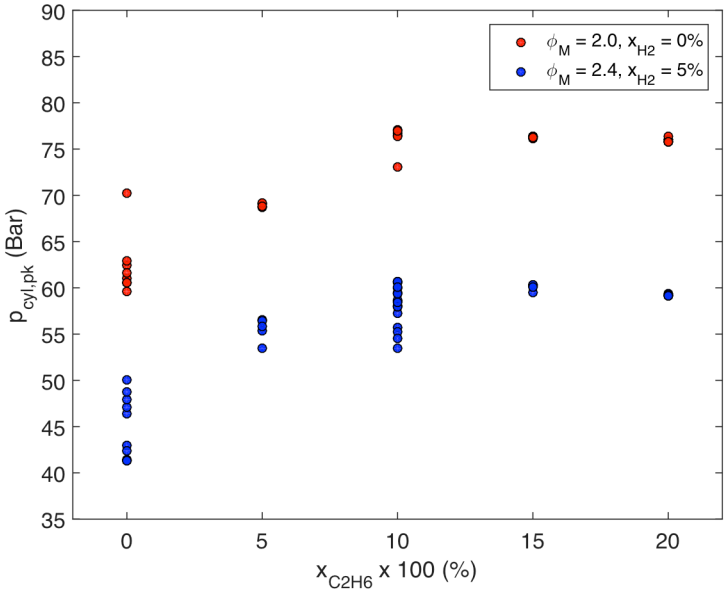

Figure 15. Average peak cylinder pressure ($p_{cyl,pk}$) for different concentrations of C_2H_6 in CH_4 ($x_{C_2H_6}$, expressed as a percentage) from 0% to 20%. Comparison shown for $\phi_M = 2.0$ ($x_{H_2} = 0\%$) and 2.4 ($x_{H_2} = 5\%$) with different values of $x_{C_2H_6}$. Each point corresponds to an average of 200 consecutive engine cycles.

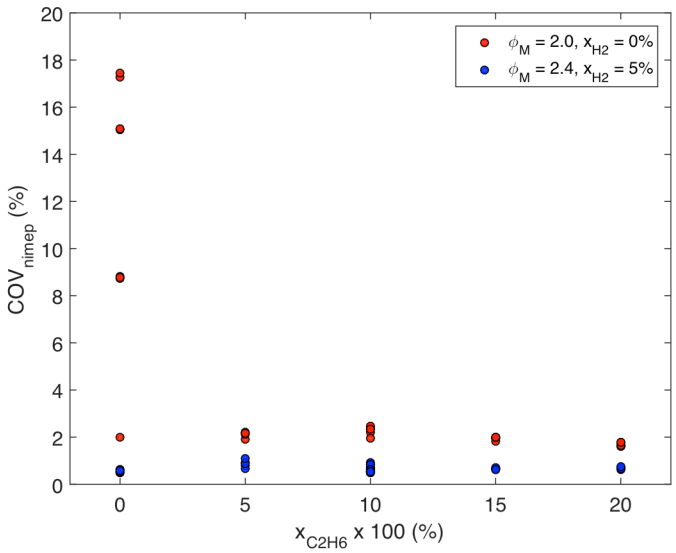

Figure 16. Coefficient of variation of $nimep$ (COV_{nimep}) for different concentrations of C_2H_6 in CH_4 ($x_{C_2H_6}$, expressed as a percentage) from 0% to 20%. Comparison shown for $\phi_M = 2.0$ ($x_{H_2} = 0\%$) and 2.4 ($x_{H_2} = 5\%$) with different values of $x_{C_2H_6}$. Each point corresponds to an average of 200 consecutive engine cycles.

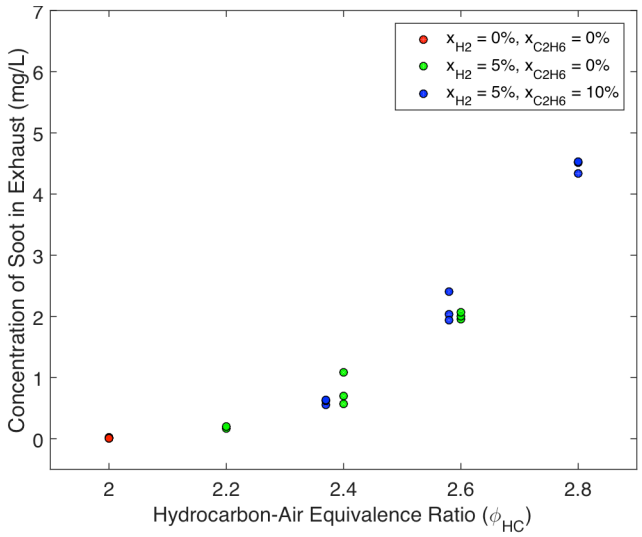

Figure 17. Soot concentration in exhaust gases, measured gravimetrically, at hydrocarbon-air equivalence ratios ϕ_{HC} = 2.0 to 2.8, contrasting the effects of H_2 and C_2H_6.

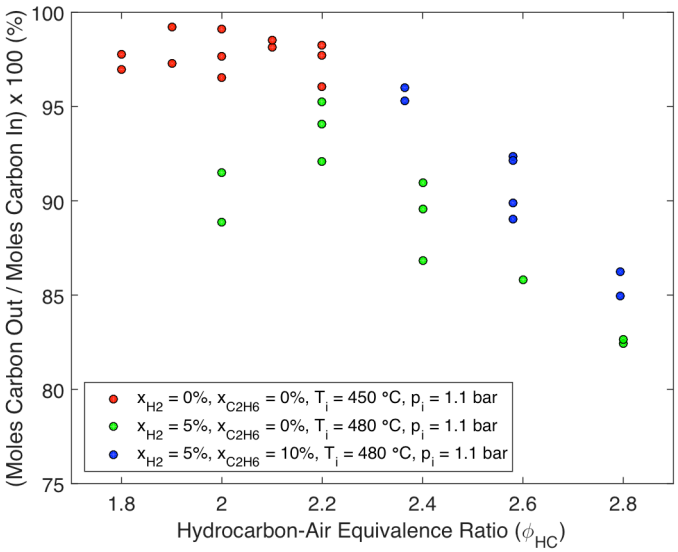

Figure 18. Carbon balance through engine, at hydrocarbon-air equivalence ratios ϕ_{HC} = 1.8 to 2.8.

References

1. U.S. Energy Information Administration (2011) “Over one-third of natural gas produced in North Dakota is flared or otherwise not marketed.”
2. U.S. Energy Information Administration (2010) “United States Total Distribution of Wells by Production Rate Bracket.”
3. Fleisch, T.H., Basu, A., and Sills, R.A. (2012) Introduction and advancement of a new clean global fuel: The status of DME developments in China and beyond. *J. Nat. Gas Sci. Eng.* **9**, 94–107.
4. (1985) “3.5.4.1 Partial Oxidation of Oil and Gas Feedstocks”, *Ullmanns Encycl. Ind. Chem.* A2, 213–215.
5. Enger, B.C., Lødeng, R., and Holmen, A. (2008) A review of catalytic partial oxidation of methane to synthesis gas with emphasis on reaction mechanisms over transition metal catalysts. *Appl. Catal. Gen.* **346** (1), 1–27.
6. Acocella, A., Lim, E., Cedrone, K., et al. (2014) “System and Market Analysis of Methanol Production Using Compact Engine Reformers”, *ASME 2014 8th Int. Conf. Energy Sustain. Collocated ASME 2014 12th Int. Conf. Fuel Cell Sci. Eng. Technol.*, V002T03A005–V002T03A005.
7. Royal Dutch Shell “Pearl GTL.”
8. Ron Sills “The Dawn of DME as a Transportation Fuel in North America.”
9. “Production Units”, *Oberon Fuels*.
10. The Linde Group (2007) “Additional Technologies.”
11. Gas Technologies LLC “The GasTechno® Process.”
12. Rostrup-Nielsen, J., and Christiansen, L.J. (2011) *Concepts in Syngas Manufacture*, World Scientific.
13. Malin, J.B. (1951) “Engine generation of synthesis gas,” US2543791 A.
14. Otto, H. (1958) “Internal combustion engine for the production of synthesis gas,” US2846297 A.
15. Oberdorfer, J.P.E. (1960) “Partial oxidation of methane in a motored engine,” US2922809 A.
16. III, L.B., Green, W.H., Sappok, A., et al. (2014) “Engine Reformer Systems For Lower Cost, Smaller Scale Manufacturing Of Liquid Fuels,” US20140144397 A1.
17. Ghazi A. Karim, I.W. (2008) The production of hydrogen through the uncatalyzed partial oxidation of methane in an internal combustion engine. *Int. J. Hydrog. Energy* (8), 2105–2110.
18. Karim, G.A., and Moore, N.P.W. (1990) “The Production of Hydrogen by the Partial Oxidation of Methane in a Dual Fuel Engine,” 901501.
19. Karim, G.A., and Moore, N.P.W. (1990) “Examination of Rich Mixture Operation of a Dual Fuel Engine,” 901500.
20. Hiratsuka, Y. (1963) “Production of synthesis gas by an internal combustion engine.”
21. Ghaffarpour, M., Lock, A., and Shojaeefard, M. (2004) “Partial Oxidation of Natural Gas Using Internal Combustion Engines,” 2004-01-0621.
22. McMillian, M.H., and Lawson, S.A. (2006) Experimental and modeling study of hydrogen/syngas production and particulate emissions from a natural gas-fueled partial oxidation engine. *Int. J. Hydrog. Energy* **31** (7), 847–860.
23. Goodwin, D.G. (2003) An open-source, extensible software suite for CVD process simulation. *Chem. Vap. Depos. XVI EUROCVD* **14** (40), 2003–08.

24. Wang, H., You, X., Joshi, A. V., Davis, S. G., Laskin, A., Egolfopoulos, F. N., and Law, C. (2007) *USC Mech Version II. High-Temperature Combustion Reaction Model of H2/CO/C1-C4 Compounds*.
25. Heywood, J. (1988) *Internal Combustion Engine Fundamentals*, McGraw-Hill Education.
26. Chaudhuri, S., Wu, F., and Law, C.K. (2013) Scaling of turbulent flame speed for expanding flames with Markstein diffusion considerations. *Phys. Rev. E Stat. Nonlin. Soft Matter Phys.* **88** (3), 033005.
27. Kochar, Y., Seitzman, J., Lieuwen, T., et al. (2011) Laminar Flame Speed Measurements and Modeling of Alkane Blends at Elevated Pressures With Various Diluents., 129–140.
28. Dugger, G.L. (1952) *Effect of Initial Mixture Temperature on Flame Speed of Methane-air, Propane-air and Ethylene-air Mixtures*, National Advisory Committee for Aeronautics.
29. Duggal, V.K., Priede, T., and Khan, I.M. (1978) "A Study of Pollutant Formation within the Combustion Space of a Diesel Engine," 780227.
30. "e-CFR: Title 40: Protection of Environment PART 1039—CONTROL OF EMISSIONS FROM NEW AND IN-USE NONROAD COMPRESSION-IGNITION ENGINES Subpart B—Emission Standards and Related Requirements", *Electron. Code Fed. Regul.* Title 40: Protection of Environment PART 1039—CONTROL OF EMISSIONS FROM NEW AND IN-USE NONROAD COMPRESSION-IGNITION ENGINES Subpart B—Emission Standards and Related Requirements.
31. Lignell, D.O., Chen, J.H., Smith, P.J., et al. (2007) The effect of flame structure on soot formation and transport in turbulent nonpremixed flames using direct numerical simulation. *Combust. Flame* **151** (1–2), 2–28.